



OPEN ACCESS

EDITED BY
Xiaohui Gao,
Central South University, China

REVIEWED BY
Yuhui Peng,
Nanchang Hangkong University, China
Jun He,
Hunan Institute of Engineering, China

*CORRESPONDENCE
Bingzhen Li,
tylerlibz@hotmail.com
Qingqing Wu,
164362808@qq.com
Jinlong Zhao,
zjl767688612@163.com

SPECIALTY SECTION
This article was submitted to
Catalytic Reactions and Chemistry,
a section of the journal
Frontiers in Chemistry

RECEIVED 16 November 2022
ACCEPTED 22 November 2022
PUBLISHED 09 January 2023

CITATION
Wang J, Chen Y, Wei Y, Li Y, Li F, Li B,
Wu Q and Zhao J (2023), Enhancement
of microwave absorption performance
of porous carbon induced by Ce
(CO₃) OH.
Front. Chem. 10:1100111.
doi: 10.3389/fchem.2022.1100111

COPYRIGHT
© 2023 Wang, Chen, Wei, Li, Li, Wu
and Zhao. This is an open-access article
distributed under the terms of the
[Creative Commons Attribution License
\(CC BY\)](https://creativecommons.org/licenses/by/4.0/). The use, distribution or
reproduction in other forums is
permitted, provided the original
author(s) and the copyright owner(s) are
credited and that the original
publication in this journal is cited, in
accordance with accepted academic
practice. No use, distribution or
reproduction is permitted which does
not comply with these terms.

Enhancement of microwave absorption performance of porous carbon induced by Ce (CO₃) OH

Jijun Wang^{1,2}, Yuhua Chen², Yaxing Wei², Yan Li², Fangyuan Li²,
Bingzhen Li^{2*}, Qingqing Wu^{2*} and Jinlong Zhao^{2*}

¹Chinese People's Liberation Army, Beijing, China, ²Institute of Defense Engineering, Academy of Military Sciences, Beijing, China

In recent years, electromagnetic pollution has become more and more serious, resulting in a very negative impact on people's health. Therefore, it is important to develop efficient microwave absorbers to reduce electromagnetic pollution. Here, we construct a novel absorbing material of the polymer gel-derived porous carbon decorated by rare earth compounds (Ce (CO₃) OH). When the thickness is 2.2 mm, the composite exhibits excellent microwave absorption performance with the optimal RL_{min} value and EAB reached up to -47.67 dB and 5.52 GHz, respectively, covering the Ku band. The high-efficiency microwave absorption is mainly attributed to the synergistic effect of dipole polarization, defect polarization and interfacial polarization. This work not only provides a new view for designing superior absorber materials, but also lay a foundation for their real applications.

KEYWORDS

microwave absorbers, impedance matching, rare earth compounds (Ce (CO₃) OH), Ce (CO₃) OH/C composite, synergistic effect

1 Introduction

With the widespread use of electronic equipment in our daily lives, microwave absorbers have become totally essential to protect human health from serious electromagnetic pollution and improve the apparatus' communication signal quality (Xu et al., 2019; Zhang et al., 2020; Wang et al., 2021; Nan et al., 2022). So far, much effort have been devoted into the development of target absorbers and the core requirements were identified as light weight, strong absorption, thin layer and broad bandwidth (Phang et al., 2008; Wan et al., 2015; Mo et al., 2019). To achieve these goals, various nano-structural materials have been reported, including magnetic metal oxides (Liu et al., 2013; Zhou et al., 2015), MXene (Han et al., 2017; Huang et al., 2022a), metal alloy (Lutsev and Shutkevich, 2016; Xu et al., 2018; Huang et al., 2022b) and carbonaceous substances (Wu et al., 2021; Wu et al., 2022), etc. Among them, carbon-based nanomaterials derived from gel structure attracted much attention as a result of low density, abundant porosity and adjustable dielectric property (Wang

et al., 2022a). By using agar gel containing NiCO_3 as precursors, Guo et al. synthesized a Ni/C composite consisting of three-dimensional carbon structure with accommodated nickel nanoparticles, which showed an excellent absorbing capability with a broad bandwidth in the range of 13.2 GHz–18 GHz. (Xie et al., 2018). Sun et al. proposed different magnetic metals and porous carbon composite structure on the basis of sol-gel method and subsequent *in situ* pyrolysis process. The prepared composites provided multiple loss pathway of electromagnetic wave and the minimum value of reflection loss was -33.5 dB at 7.7 GHz (Shen et al., 2022). Combining a typical sol-gel approach with supercritical drying and carbonization process, Yang et al. reported a resorcinol-formaldehyde based carbon aerogel with pore structure and good impedance matching. The wide effective bandwidth was estimated to be 4.5 GHz and minimum reflection loss value was determined to be -37.5 dB (Wang et al., 2022b). It follows that further improvement of absorbing performance from gel-derived carbonaceous materials is still limited by the narrow effective bandwidth, which may hinder their practical applications.

In recent, optimization of impedance matching has gradually been proved to expand the absorption bandwidth, and then increase electromagnetic wave attenuation performance (Rehman et al., 2019; Qiao et al., 2020; Jin et al., 2022). Several strategies have been proposed to regulate the dielectric properties of carbon materials, realizing the broadband and strong absorption (Wang et al., 2022c; He et al., 2022; Xu et al., 2022). For example, to reach a minimum reflection loss of -61.2 dB and an effective absorption bandwidth covering 5.2 GHz, Zhu et al. constructed a tubular structured carbon nanofibers coated with titanium dioxide layers, which showed the wave-transparent behavior to change the complex permittivity of carbonaceous constituent and facilitate the composites' impedance matching (Kang et al., 2020). Similarly, Che et al. optimized the conductivity by anchoring the carbon nanotubes on TiO_2 nanospheres or designing a multiple structure of vesicle-like-shell TiO_2 @carbon *via* the pyrolyzing the bimetallic zeolitic imidazolate framework encapsulating TiO_2 nanoparticles or metal-polydopamine-coated TiO_2 , respectively. The obtained absorption performance presented a reflection loss of -44.0 dB and an effective absorption bandwidth of 5.4 GHz at the thickness of 2.0 mm (Ding et al., 2020). To improve its poor impedance-matching characteristic, Zhang et al. modified the ordered mesoporous carbon with silica (OMC-5@ SiO_2) through a self-assemble method and heat treatment process. With the impedance ratio around 1 from 8.56 GHz to 13.2 GHz, the OMC-5@ SiO_2 reached an effective absorption bandwidth of 4.8 GHz and the minimum reflection value of -40.7 dB at 10.8 GHz (Zhou et al., 2020). Nevertheless, the reported strategies are still limited, and new approaches are expected.

In this work, a new composite consisting of the polymer gel-derived porous carbon decorated by rare earth compounds [$\text{Ce}(\text{CO}_3)\text{OH}$] was designed and synthesized. Compared to pure carbon materials, the prepared composites [$\text{Ce}(\text{CO}_3)\text{OH}/\text{C}$] presented the significant higher pyrrolic N and 1.02 I_D/I_G value. The electromagnetic parameters analysis showed that the modified composites' conductivity occurred downshift with the filling ratio of 10% and the thickness of 1.85 mm. For the electromagnetic wave absorption, by changing the absorbers' thickness to 2.2 mm, the optimal RL_{min} value and EAB reached up to -47.67 dB and 5.52 GHz, respectively, covering the Ku band. It is believed that the results reported in this work will not only provide a new thought for controlling the impedance matching for carbon-based materials, but also lay a foundation for their real applications.

2 Experimental section

2.1 Materials

The P123 (PEO-PPO-PEO) material was purchased from sigma-Aldrich. The hexamethylenetetramine ($\text{C}_6\text{H}_{12}\text{N}_4$) and hydrochloric acid (HCl) were bought from Sinopharm Group. The 2,4-dihydroxybenzoic acid ($\text{C}_7\text{H}_6\text{O}_4$) and cerium nitrate hexahydrate ($\text{Ce}(\text{NO}_3)_2 \cdot 6\text{H}_2\text{O}$) were purchased from Aladdin Reagent. The ethylenediamine was bought from General Reagent. All chemicals were utilized without further purification.

2.2 Preparation of polymer gel

Firstly, 3.56 g P123 was dissolved in 60 ml deionized water and sonicated for 30 min. Then, 0.936 g hexamethylenetetramine, 3.115 g 2,4-dihydroxybenzoic acid and 415 μl ethylenediamine were added into the above solution, sonicated and dispersed, and transferred to a 100 Teflon-lined stainless autoclave and heated at 130°C for 4 h. Finally, orange-red product was filtered and washed, and dried in a freeze dryer for 24 h.

2.3 Preparation of carbon materials

First, 1 g of polymer gel and 4 g of calcium carbonate nanoparticles were well ground and calcined in a tube furnace under nitrogen atmosphere at 900°C for 2 h. Then, the calcination product was immersed in 40 ml of 3 M HCl and stirred for 1 h to remove the generated calcium oxide. Finally, the product was filtered, washed with deionized water until neutral, and dried overnight at 70°C under vacuum.

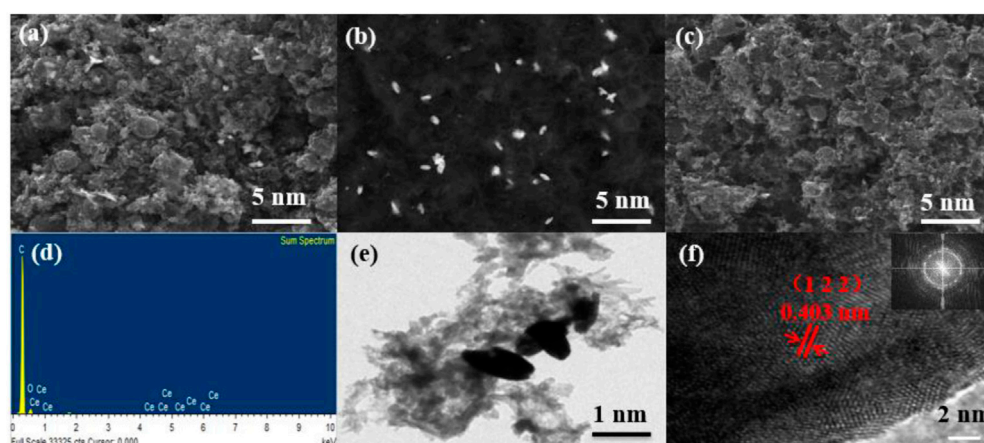


FIGURE 1

(A) Bright-field SEM picture for Ce/PC; (B) Dark field SEM picture for Ce/PC; (C) Bright-field SEM picture for PC; (D) EDS picture of Ce/PC; (E) TEM image of Ce/PC; (F) HR-TEM and SAED images of Ce/PC.

2.4 Preparation of porous carbon loaded cerium nanomaterials (Ce/PC)

First, 100 mg of the above carbon materials and 200 mg of Ce $(\text{NO}_3)_2 \cdot 6\text{H}_2\text{O}$ were added to 30 ml deionized water, sonicated for 2 h and stirred for 24 h, and then dried under vacuum for 24 h. Finally, the product was calcined at $1,000^\circ\text{C}$ for 1 h under N_2 with a heating rate of 5°C min^{-1} . In addition, the blank sample PC was obtained by direct pyrolysis of a carbon material without adsorbed Ce.

2.5 Characterization and tests

The crystal structure was measured by X-ray diffraction (Bruker, D8 Advance). The micro-morphology and micro-structure were observed by scanning electron microscope (SEM) (Tescan MIRA3 LMU) and transmission electron microscopy (TEM) (JEOL JEM-2100F). Chemical composition was studied by X-ray photoelectron spectroscopy (XPS) on a K-Alpha 1063 X-ray photoelectron spectrometer. Raman tests were recorded on Renishaw Raman spectrometer. The microwave absorption (MA) performance was investigated by a microwave vector network analyzer (VNA, Agilent N5230A).

3 Results and discussion

3.1 Structural and morphological analysis

The surface morphology and elemental composition of the prepared samples were analyzed by scanning electron

microscopy (SEM). As shown in Figures 1(A–C), there is no significant difference in the micro-morphology between Ce/PC and PC samples, which are composed of irregular bulk particles. Ce grows in porous carbon to form Ce/PC sample, which is confirmed by EDS pattern of Ce/PC sample (Figure 1D). The TEM image (Figure 1E) show granular Ce growing on a porous carbon skeleton substrate. Additionally, the related HR-TEM (Figure 1F) image for Ce/PC shows clear lattice space of 0.403 nm, which is attributed to (1 2 2) plane of Ce $(\text{CO}_3)\text{OH}$, further demonstrating the successful addition of Ce. The selected area electron diffraction (SAED) exhibits a ring-shape pattern corresponding to the Ce $(\text{CO}_3)\text{OH}$.

It can be seen from the X-ray powder diffraction (XRD) pattern in Figure 2A that both Ce/PC and PC samples have two broad diffraction peaks at 26.5° and 43.3° , which are attributed to (0 0 2) and (1 0 1) planes of carbon. The characteristic peaks of Ce/PC is the same as that of the standard comparison card PDF # 41-0013, which proves that Ce in Ce/PC sample exists in the form of Ce $(\text{CO}_3)\text{OH}$. Normally, the degree of graphitization of a material can be characterized by Raman spectroscopy. From Figure 2B, both Ce and Ce/PC exhibit two peaks located at around $1,333\text{ cm}^{-1}$ (D band) and $1,587\text{ cm}^{-1}$ (G band). The D band signifies the sp^3 defects or disorder, and G band indicates the sp^2 hybridization. The I_D/I_G is usually used to reflect the degree of disorder (Shu et al., 2018a; Wu et al., 2019). It can be seen from Figure 3B that the I_D/I_G of the prepared material decreases slightly with the doping of Ce, which indicates that the degree of defect or disorder is reduced in Ce/PC sample.

The chemical composition of PC and Ce/PC sample was determined by X-ray photoelectron spectroscopy (XPS). The peaks of C and Ce elements were found in the XPS survey spectrum of Ce/PC (Figure 3A), further confirming the

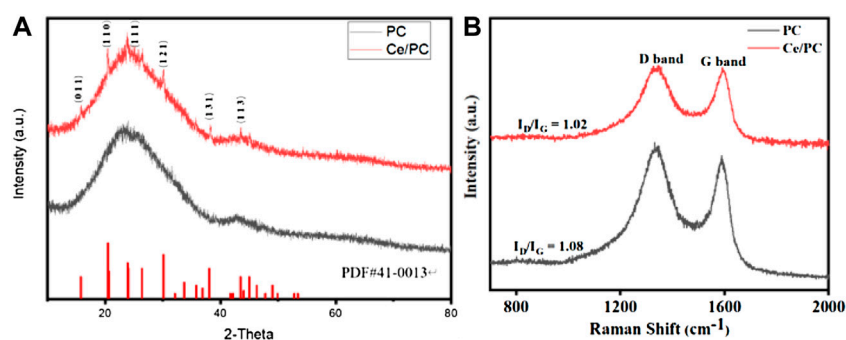


FIGURE 2
(A) XRD patterns and (B) Raman spectra for Ce/PC and PC.

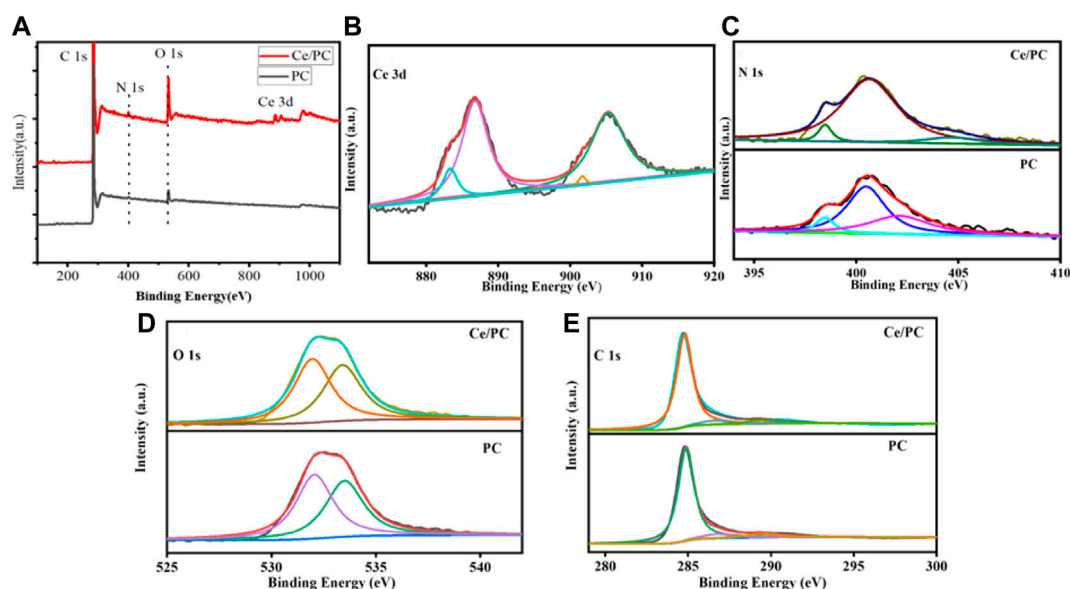
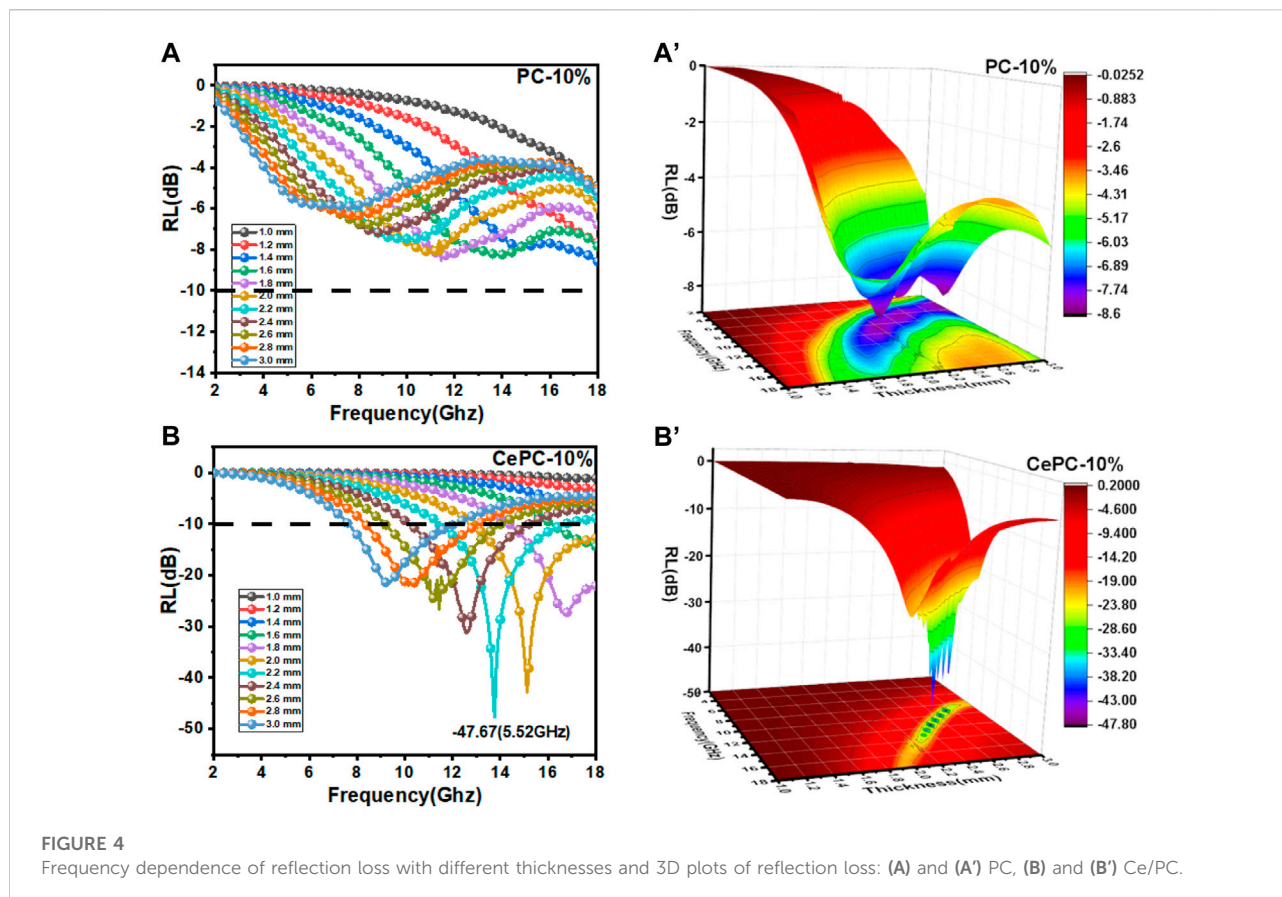


FIGURE 3
(A) XPS survey spectra for Ce/PC and PC; (B) Ce 3d XPS spectrum for Ce/PC; (C) N 1s XPS spectra, (D) O 1s XPS spectra and (E) C 1s XPS spectra for Ce/PC and PC.

presence of these elements in the Ce/PC sample. In Ce 3d spectra (Figure 3B), Ce/PC sample shows four characteristic peaks. The Ce 3d_{3/2} is marked as U and U', and Ce 3d_{5/2} is marked as V and V'. The characteristic peaks U' and V represent Ce³⁺, and the characteristic peaks U and V' represent Ce⁴⁺ (Wu et al., 2020). Therefore, Ce⁴⁺ and Ce³⁺ coexist in Ce-PC, indicating the presence of oxygen vacancies. The electric conductivity increases with the increase of oxygen vacancy defects (Shu et al., 2018a; Wu et al., 2019). The enhanced electric conductivity is beneficial

to enhancing the conduction loss and charge polarization relaxation of Ce-PC sample (Chen et al., 2020; Zhao et al., 2020). The N 1s spectra (Figure 3C) demonstrated the presence of pyridinic-N (398.4 eV), graphitic-N (400.5 eV) and oxide-N (402.1 eV, 404.7 eV) in PC and Ce/PC samples (Yang et al., 2020). From Figure 3D, the O 1s spectra can be fitted into two peaks of -COOH (531.9 eV) and -OH (533.4 eV). (Soren et al., 2016). As shown in Figure 3E, the peaks of C 1s at 289.3 eV, 286.9 eV and 284.8 eV can be assigned to O-C=O, C-O and C=N bonds, respectively.



3.2 Microwave absorption properties

The microwave absorption properties of microwave absorbing materials can be evaluated by reflection loss (RL). According to the transmission line theory, the RL is calculated by the following formula (Wang et al., 2019a; Liu et al., 2019; Luo et al., 2020):

$$R_L = 20 \lg \frac{|Z_{in} - Z_0|}{|Z_{in} + Z_0|} \quad (1)$$

$$Z_{in} = \sqrt{\frac{\mu_r}{\epsilon_r}} \tanh \left[j \frac{2\pi}{c} \sqrt{\mu_r \epsilon_r} f d \right] \quad (2)$$

Herein Z_{in} is the input impedance of absorber, Z_0 is the impedance of free space, ϵ_r is the relative complex permittivity, μ_r is the relative complex permeability, d is the thickness of the absorber, c is the velocity of light in free space, and f is the frequency.

As described in Figures 4A, 4A', the RL_{min} of PC samples is less than 10 dB, indicating that pure PC materials have weak microwave absorption properties. From Figures 4B, B', compared with PC samples, the RL_{min} of Ce/PC samples at 13.76 GHz is -47.67 dB, showing significantly improved microwave absorption properties, the corresponding thickness is 2.2 mm,

and the effective absorption bandwidth (EAB, $RL < -10$ dB) can reach 5.52 GHz. In addition, more than 10 dB can be achieved by adjusting the matching thickness from 1 mm to 3 mm, covering almost the entire Ku and X-band.

Generally, the electromagnetic parameters (ϵ' , ϵ'' , μ' , μ'') are vitally important to determine the microwave absorption properties of absorbers (Shu et al., 2018b; Shu et al., 2019a; Shu et al., 2019b). The real permittivity (ϵ') and real permeability (μ') represent the storage ability of electric and magnetic field energies, whereas the imaginary permittivity (ϵ'') and imaginary permeability (μ'') indicate the dissipation capacity of electric and magnetic field energies, respectively (Shu et al., 2018b; Shu et al., 2019a; Shu et al., 2019b). Since the material we have prepared is almost non-magnetic, only its complex permittivity is discussed here. It can be seen from Figure 5A that the ϵ' of all samples decreases with the increase of frequency, showing a dispersion behavior, which is beneficial to the attenuation of microwave energy (Quan et al., 2017). Among them, the ϵ' of PC and CePC samples decreased from 21.21 to 5.04, 10.67 to 5.83, respectively. The results show that the addition of Ce (CO_3) OH can inhibit the high dielectric behavior of PC materials and improve the properties of the materials. As shown in Figure 5B, with the increase of frequency, ϵ' and ϵ'' show a similar trend of change.

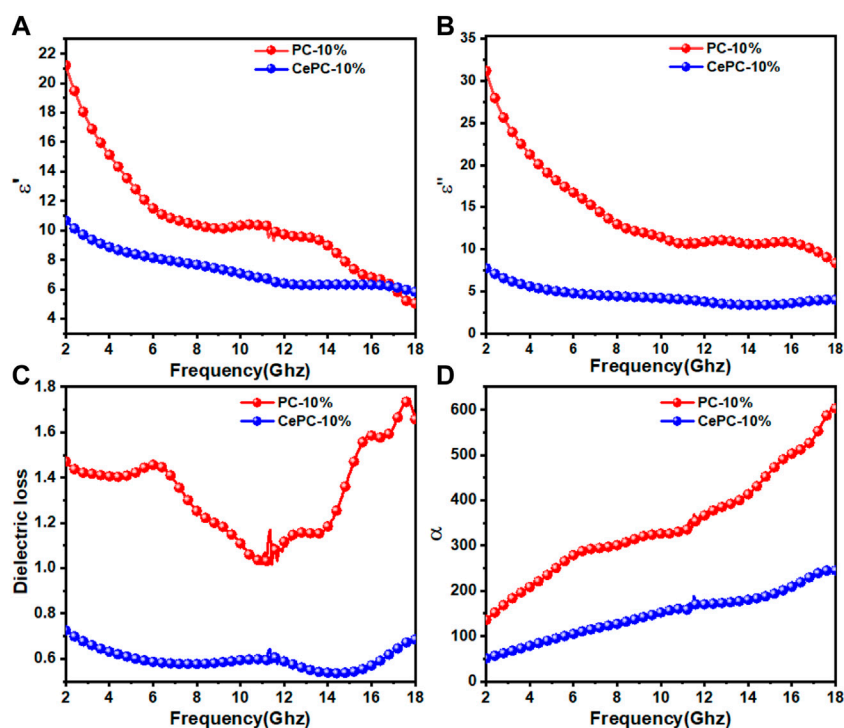


FIGURE 5

Electromagnetic parameters of PC and Ce/PC: (A) the real part and (B) the imaginary part of complex permittivity, (C) dielectric loss and (D) attenuation constant α .

According to the free electron theory, ϵ'' increases with the increase of electrical conductivity. However, pure Ce is an electrical insulator. On the contrary, the introduction of it suppresses the conductive behavior of PC materials, so the ϵ'' of Ce/PC is lower than that of PC materials. We further analyzed the dielectric loss tangent ($\tan\delta = \frac{\epsilon''}{\epsilon'}$). From Figure 5C, the $\tan\delta$ value of pure PC material is higher than that of CePC, thanks to the high ϵ'' of PC. However, due to the introduction of Ce (CO_3) OH, the $\tan\delta$ value of Ce/PC material is in the range of 0.5–0.8, which weakens the dielectric loss ability of PC to some extent.

The attenuation ability of electromagnetic wave is usually reflected by the attenuation constant (α), which can be expressed as follows (Shu et al., 2019b; Wang et al., 2019b; Shu et al., 2019c; Zhang et al., 2019):

$$\alpha = \frac{\sqrt{2}\pi f}{c} \times \sqrt{(\mu''\epsilon'' - \mu'\epsilon') + \sqrt{(\mu''\epsilon'' - \mu'\epsilon')^2 + (\mu''\epsilon' + \mu'\epsilon'')^2}} \quad (3)$$

Figure 5D shows the frequency dependence of the attenuation constant α of the prepared samples. As can be seen from Figure 5D, compared with PC materials, Ce/PC shows relatively weak electromagnetic wave attenuation ability. The

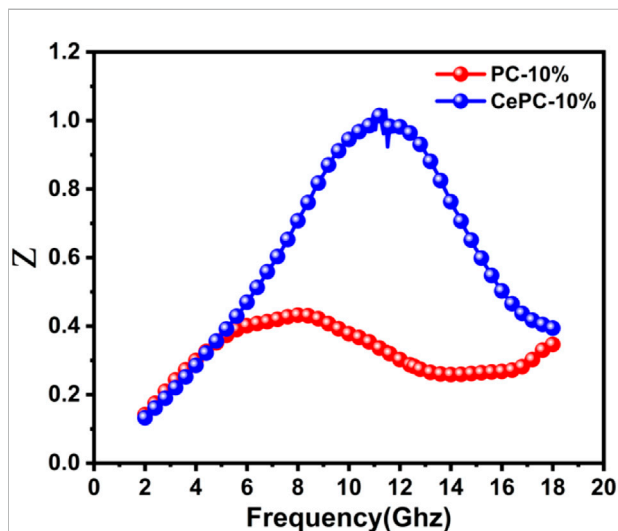


FIGURE 6

Frequency dependence of normalized impedance matching (Z) for the samples of PC and Ce/PC.

change of attenuation capacity mainly comes from the change of dielectric loss. However, PC does not show the best microwave absorption performance, as shown in Figure 4. Therefore, the

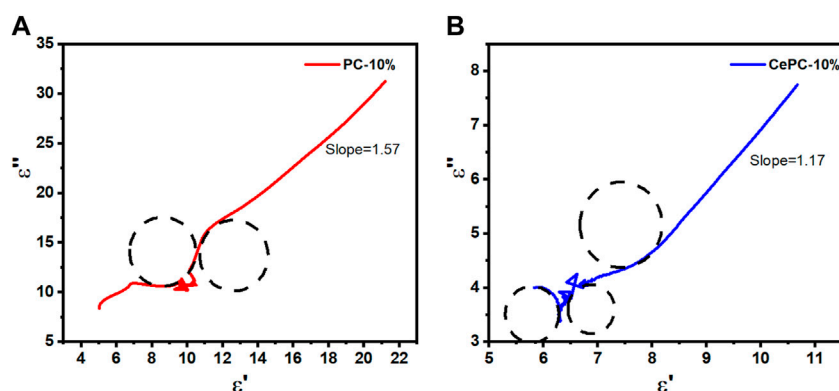


FIGURE 7 Cole–Cole semicircle ($\epsilon'' \sim \epsilon'$) curves of the samples: (A) PC, (B) Ce/PC.

impedance matching characteristics need to be further considered.

As shown in Figure 6, the Z value of pure PC material is far from 1, which indicates that the impedance matching is poor. The Ce/PC material is closer to the optimal impedance matching line ($Z = 1$), which indicates that the impedance matching has been greatly improved. Due to the realization of the best impedance matching, most of the incident microwaves can enter the material (Liu et al., 2017a; Wang et al., 2019c). At the same time, the moderate electromagnetic attenuation ability can effectively convert electromagnetic energy into thermal energy (Shu et al., 2019a; Wang et al., 2019c; Zhang et al., 2019). Therefore, Ce/PC shows better microwave absorption properties.

According to Debye theory, dielectric loss includes conduction loss and polarization loss (Liu et al., 2017b). ϵ' and ϵ'' follow the equation (Liu et al., 2017b; Shu et al., 2018b; Shu et al., 2019b):

$$\left(\epsilon' - \frac{\epsilon_{\infty} + \epsilon_s}{2}\right) + (\epsilon'')^2 = \left(\frac{\epsilon_{\infty} - \epsilon_s}{2}\right)^2 \quad (4)$$

Herein, ϵ_s , ϵ_{∞} , ϵ' and ϵ'' are the static permittivity, relative dielectric permittivity at high-frequency limit, real part and imaginary part of permittivity, respectively (Liu et al., 2017b; Shu et al., 2018b; Shu et al., 2019b). Based on Eq. 4, the curve of ($\epsilon'' \sim \epsilon'$) should be a single semicircle, which is known as Cole–Cole semicircle (Liu et al., 2017b; Shu et al., 2018b; Shu et al., 2019b). Each semicircle represents a Debye relaxation process (Liu et al., 2017b; Shu et al., 2018b; Shu et al., 2019b). Figures 7A,B shows the Cole–Cole diagram of sample PC and Ce/PC. From Figures 7A,B, PC and Ce/PC show two and three semicircles, respectively, indicating that Ce/PC materials have more relaxation processes. This is mainly due to the increase of internal defects caused by the introduction of Ce (CO₃) OH, which leads to the increase of polarization relaxation of defect

dipoles, which can be obtained by further analysis of XPS and Raman spectra. In addition, it can be observed that the semicircle is deformed to a certain extent, and the Cole–Cole diagram has a part of the tail straight line region, which indicates that Debye relaxation is not the only mechanism of dielectric loss, and other mechanisms such as conductive loss may be the cause of microwave absorption (Shu et al., 2018b; Shu et al., 2018c). By fitting the straight line part of the Cole–Cole diagram, the slopes are 1.57 and 1.17 respectively, which indicates that the conductive loss plays a more important role in PC materials.

We analyzed the possible microwave absorption mechanism of Ce (CO₃) OH/C nanocomposites. First of all, under the action of alternating electromagnetic field, the residual groups (-COOH and -OH) and structural defects on the surface or edge of porous carbon will cause dipole polarization and defect polarization (Suresh et al., 2013; Shu et al., 2018a), respectively. At the same time, Ce (CO₃) OH nanoparticles can also be used as polarization centers to further enhance dipole polarization relaxation (Wu et al., 2019). Secondly, a large number of heterogeneous interfaces between paraffin matrix, porous carbon and Ce (CO₃) OH can arrange polar bonds or charges under the action of alternating electromagnetic field to attenuate the power of incident microwave, like the same kind of capacitor structure (Cao et al., 2012). Third, according to Cao's electron hopping model (Song et al., 2009; Cao et al., 2010), electrons can absorb electromagnetic energy and migrate on the porous carbon surface, and Ce (CO₃) OH nanoparticles can be used as a bridge for electron hopping, thus improving the conductive loss, and further converting electromagnetic energy into thermal energy through collision with the lattice (Cao et al., 2018).

As shown in Table 1, we summarize the literature on Ce (CO₃) OH/C composites as microwave absorbing materials and Ce as filling materials reported in this work (Wang et al., 2016; Xing et al., 2017; Ge et al., 2019). Obviously, among the reported Ce filled carbon matrix composites, the prepared Ce (CO₃) OH/C

TABLE 1 Typical Ce-based composites as microwave absorbers reported in this work and recent literatures.

Samples	Matrix	RL _{min} (dB)	EAB (GHz)	Thickness (mm)	Ref
Ce (CO ₃) OH/C	Paraffin	-47.67	5.52	2.2	This work
PANI/CeO ₂ nanocomposite	Paraffin	-40.0	4.0	3.0	Xing et al. (2017)
CeO ₂ /Fe ₃ O ₄ composite	Paraffin	-28.9	—	7.8	Wang et al. (2016)
CeO ₂ /Fe composite	Paraffin	-17.0	4.24	1.24	Ge et al. (2019)

nanocomposites have good microwave absorption properties, strong absorption and thin thickness.

4 Conclusion

In summary, a new composite material composed of porous carbon derived from polymer gel decorated with rare earth compound [Ce (CO₃) OH] was successfully synthesized by one-pot hydrothermal method. The results show that compared with pure carbon materials, the prepared composites [Ce (CO₃) OH/C] show significantly higher pyrroline N value, and the dispersion of the particles is better. In addition, the introduction of Ce (CO₃) OH can improve the impedance matching of porous carbon materials, which has a significant effect on electromagnetic parameters and microwave absorption properties. When the filling ratio is 10 wt%, the prepared nanocomposites exhibit the best RL of -47.67 dB and EAB of 5.52 GHz at a thickness of only 2.2 mm. By adjusting the matching thickness from 1 mm to 3 mm, the matching thickness can be below 10 dB, covering almost the entire Ku and X-band. In addition, the possible microwave absorption mechanism of nanocomposites is proposed, which can be attributed to the synergistic effect of dipole polarization, defect polarization and interfacial polarization. In addition, the conductive loss is increased due to electron migration. Therefore, the prepared nanocomposites can be used as efficient absorbing materials in the field of electromagnetic wave absorption.

References

- Cao, M., Wang, X., Cao, W., Fang, X., Wen, B., and Yuan, J. (2018). Thermally driven transport and relaxation switching self-powered electromagnetic energy conversion. *Small* 14, 1800987. doi:10.1002/smll.201800987
- Cao, M-S., Song, W-L., Hou, Z-L., Wen, B., and Yuan, J. (2010). The effects of temperature and frequency on the dielectric properties, electromagnetic interference shielding and microwave-absorption of short carbon fiber/silica composites. *Carbon* 48, 788–796. doi:10.1016/j.carbon.2009.10.028
- Cao, M-S., Yang, J., Song, W-L., Zhang, D. Q., Wen, B., Jin, H. B., et al. (2012). Ferroferric oxide/multiwalled carbon nanotube vs polyaniline/ferroferric oxide/multiwalled carbon nanotube multiheterostructures for highly effective microwave absorption. *ACS Appl. Mat. Interfaces* 4, 6949–6956. doi:10.1021/am3021069
- Chen, W. S., Xue, J., Bao, Y. F., and Feng, L. (2020). Surface engineering of nanoceria facet dependent coupling effect on Pt nanocrystals for electro-catalysis of

Data availability statement

The original contributions presented in the study are included in the article/Supplementary Material, further inquiries can be directed to the corresponding authors.

Author contributions

JW: Material preparation, electrochemical measurements, data analysis, writing-original draft. YC: tests. YW: measurements. YL: analysis. FL: analysis. BL: review. QW: review. JZ: Review.

Conflict of interest

The authors declare that the research was conducted in the absence of any commercial or financial relationships that could be construed as a potential conflict of interest.

Publisher's note

All claims expressed in this article are solely those of the authors and do not necessarily represent those of their affiliated organizations, or those of the publisher, the editors and the reviewers. Any product that may be evaluated in this article, or claim that may be made by its manufacturer, is not guaranteed or endorsed by the publisher.

methanol oxidation reaction. *Chem. Eng. J.* 381, 122752. doi:10.1016/j.cej.2019.122752

Ding, J. J., Wang, L., Zhao, Y. H., Yu, X., Xing, L., Ding, G., et al. (2020). Rutile TiO₂ nanoparticles encapsulated in a zeolitic imidazolate framework-derived hierarchical carbon framework with engineered dielectricity as an excellent microwave absorber. *ACS Appl. Mat. Interfaces* 12, 48140–48149. doi:10.1021/acsami.0c12764

Ge, C., Wang, L., Liu, G., and Chen, H. (2019). Synthesis and electromagnetic absorption properties of CeO₂@Fe composites with core-shell structure. *J. Magnetism Magnetic Mater.* 485, 228–235. doi:10.1016/j.jmmm.2019.04.087

Han, M. K., Yin, X. W., Li, X. L., Anasori, B., Zhang, L., Cheng, L., et al. (2017). Laminated and two-dimensional carbon-supported microwave absorbers derived from mxenes. *ACS Appl. Mat. Interfaces* 9, 20038–20045. doi:10.1021/acsami.7b04602

- He, M., Liao, Q., Zhou, Y. M., Song, Z., Wang, Y., Feng, S., et al. (2022). Lightweight TiO₂@C/carbon fiber aerogels prepared from tii3c2tx/cotton for high-efficiency microwave absorption. *Langmuir* 38, 945–956. doi:10.1021/acs.langmuir.1c02237
- Huang, M. Q., Wang, L., Liu, Q., You, W., and Che, R. (2022). Interface compatibility engineering of multi-shell Fe@c@ TiO₂@MoS₂ heterojunction expanded microwave absorption bandwidth. *Chem. Eng. J.* 429, 132191. doi:10.1016/j.cej.2021.132191
- Huang, Y. F., Xie, Y. L., Zhao, J., Yin, X., and Chai, C. (2022). Variety of zif-8/Mxene-based lightweight microwave-absorbing materials: Preparation and performances of zno/mxene nanocomposites. *J. Phys. Chem. C* 126, 13847–13853. doi:10.1021/acs.jpcc.2c04026
- Jin, C., Wu, Z. C., Yang, C. D., Wang, L., Zhang, R., Xu, H., et al. (2022). Impedance amelioration of coaxial-electrospun TiO₂@Fe/C@ TiO₂ vesicular carbon microtubes with dielectric-magnetic synergy toward highly efficient microwave absorption. *Chem. Eng. J.* 433, 133640. doi:10.1016/j.cej.2021.133640
- Kang, S., Qiao, S. Y., Cao, Y. T., Hu, Z., Yu, J., Wang, Y., et al. (2020). Hyper-cross-linked polymers-derived porous tubular carbon nanofibers@ TiO₂ toward a wide-band and lightweight microwave absorbent at a low loading content. *ACS Appl. Mat. Interfaces* 12, 46455–46465. doi:10.1021/acsami.0c11839
- Liu, J. W., Xu, J. J., Che, R. C., Chen, H., Liu, M., and Liu, Z. (2013). Hierarchical Fe₃O₄@TiO₂ yolk-shell microspheres with enhanced microwave-absorption properties. *Chem. Eur. J.* 19, 6746–6752. doi:10.1002/chem.201203557
- Liu, P., Zhang, Y., Yan, J., Huang, Y., Xia, L., and Guang, Z. (2019). Synthesis of lightweight n-doped graphene foams with open reticular structure for high-efficiency electromagnetic wave absorption. *Chem. Eng. J.* 368, 285–298. doi:10.1016/j.cej.2019.02.193
- Liu, Q., Liu, X., Feng, H., Shui, H., and Yu, R. (2017). Metal organic framework-derived Fe/carbon porous composite with low Fe content for lightweight and highly efficient electromagnetic wave absorber. *Chem. Eng. J.* 314, 320–327. doi:10.1016/j.cej.2016.11.089
- Liu, W., Shao, Q., Ji, G., Liang, X., Cheng, Y., Quan, B., et al. (2017). Metal-organic-frameworks derived porous carbon-wrapped Ni composites with optimized impedance matching as excellent lightweight electromagnetic wave absorber. *Chem. Eng. J.* 313, 734–744. doi:10.1016/j.cej.2016.12.117
- Luo, J., Zhang, K., Cheng, M., Gu, M., and Sun, X. (2020). MoS₂ spheres decorated on hollow porous ZnO microspheres with strong wideband microwave absorption. *Chem. Eng. J.* 380, 122625. doi:10.1016/j.cej.2019.122625
- Lutsev, L., and Shutkevich, V. (2016). Sharp increase of microwave absorption in nonequilibrium Mn₂N- and Ni₂N-nanoferrites. *J. Phys. D: Appl. Phys.* 49, 505002. doi:10.1088/0022-3727/49/50/505002
- Mo, Z. C., Yang, R. L., Lu, D. W., Yang, L., Hu, Q., Li, H., et al. (2019). Lightweight, three-dimensional carbon nanotube@ TiO₂ sponge with enhanced microwave absorption performance. *Carbon* 144, 433–439. doi:10.1016/j.carbon.2018.12.064
- Nan, H. Y., Luo, F., Jia, H. Y., Deng, H., Qing, Y., Huang, Z., et al. (2022). Balancing between polarization and conduction loss toward strong electromagnetic wave absorption of hard carbon particles with morphology heterogeneity. *ACS Appl. Mat. Interfaces* 14, 19836–19846. doi:10.1021/acsami.2c01171
- Phang, S. W., Tadokoro, M., Watanabe, J., and Kuramoto, N. (2008). Synthesis, characterization and microwave absorption property of doped polyaniline nanocomposites containing TiO₂ nanoparticles and carbon nanotubes. *Synth. Met.* 158, 251–258. doi:10.1016/j.synthmet.2008.01.012
- Qiao, J., Zhang, X., Xu, D. M., Kong, L., Lv, L., Yang, F., et al. (2020). Design and synthesis of TiO₂/Co/carbon nanofibers with tunable and efficient electromagnetic absorption. *Chem. Eng. J.* 380, 122591. doi:10.1016/j.cej.2019.122591
- Quan, B., Liang, X., Xu, G., Cheng, Y., Zhang, Y., Liu, W., et al. (2017). A permittivity regulating strategy to achieve high-performance electromagnetic wave absorbers with compatibility of impedance matching and energy conservation. *New J. Chem.* 41, 1259–1266. doi:10.1039/c6nj03052a
- Rehman, S. U., Liu, J., Fang, Z. B., Wang, J., Ahmed, R., Wang, C., et al. (2019). Heterostructured TiO₂/C/Co from zif-67 frameworks for microwave-absorbing nanomaterials. *ACS Appl. Nano Mat.* 2, 4451–4461. doi:10.1021/acsanm.9b00841
- Shen, Z. T., Zu, Y. P., Chen, Y. Q., Ma, S., Zhang, Z., Gong, J., et al. (2022). A novel synthesis method of magnetic porous carbon composites for microwave absorption. *Synth. Met.* 291, 117184. doi:10.1016/j.synthmet.2022.117184
- Shu, R., Li, W., Wu, Y., Zhang, J., and Zhang, G. (2019). Nitrogen-doped Co-C/MWCNTs nanocomposites derived from bimetallic metal-organic frameworks for electromagnetic wave absorption in the x-band. *Chem. Eng. J.* 362, 513–524. doi:10.1016/j.cej.2019.01.090
- Shu, R., Li, W., Wu, Y., Zhang, J., Zhang, G., and Zheng, M. (2019). Fabrication of nitrogen-doped cobalt oxide/cobalt/carbon nanocomposites derived from heterobimetallic zeolitic imidazolate frameworks with superior microwave absorption properties. *Compos. Part B Eng.* 178, 107518. doi:10.1016/j.compositesb.2019.107518
- Shu, R., Li, W., Zhou, X., Tian, D., Zhang, G., Gan, Y., et al. (2018). Facile preparation and microwave absorption properties of RGO/MWCNTs/ZnFe₂O₄ hybrid nanocomposites. *J. Alloys Compd.* 743, 163–174. doi:10.1016/j.jallcom.2018.02.016
- Shu, R., Wu, Y., Li, Z., Zhang, J., Wan, Z., Liu, Y., et al. (2019). Facile synthesis of cobalt-zinc ferrite microspheres decorated nitrogen-doped multi-walled carbon nanotubes hybrid composites with excellent microwave absorption in the x-band. *Compos. Sci. Technol.* 184, 107839. doi:10.1016/j.compscitech.2019.107839
- Shu, R., Zhang, G., Wang, X., Gao, X., Wang, M., Gan, Y., et al. (2018). Fabrication of 3d net-like MWCNTs/ZnFe₂O₄ hybrid composites as high-performance electromagnetic wave absorbers. *Chem. Eng. J.* 337, 242–255. doi:10.1016/j.cej.2017.12.106
- Shu, R., Zhang, G., Zhang, J., Wang, X., Wang, M., Gan, Y., et al. (2018). Fabrication of reduced graphene oxide/multi-walled carbon nanotubes/zinc ferrite hybrid composites as high-performance microwave absorbers. *J. Alloys Compd.* 736, 1–11. doi:10.1016/j.jallcom.2017.11.084
- Song, W.-L., Cao, M.-S., Hou, Z.-L., Fang, X. Y., Shi, X. L., and Yuan, J. (2009). High dielectric loss and its monotonic dependence of conducting-dominated multiwalled carbon nanotubes/silica nanocomposite on temperature ranging from 373 to 873 k in x-band. *Appl. Phys. Lett.* 94, 233110. doi:10.1063/1.3152764
- Soren, S., Mohapatra, B. D., Mishra, S., Debnath, A. K., Aswal, D. K., Varadwaj, K. S. K., et al. (2016). Nano ceria supported nitrogen doped graphene as a highly stable and methanol tolerant electrocatalyst for oxygen reduction. *RSC Adv.* 6, 77100–77104. doi:10.1039/c6ra13218a
- Suresh, R., Ponnuswamy, V., and Mariappan, R. (2013). Effect of annealing temperature on the microstructural, optical and electrical properties of CeO₂ nanoparticles by chemical precipitation method. *Appl. Surf. Sci.* 273, 457–464. doi:10.1016/j.apsusc.2013.02.062
- Wan, G. P., Yu, L., Peng, X. G., Wang, G., Huang, X., Zhao, H., et al. (2015). Preparation and microwave absorption properties of uniform tio2@c core-shell nanocrystals. *RSC Adv.* 5, 77443–77448. doi:10.1039/c5ra14344f
- Wang, B. L., Fu, Y. G., Li, J., and Liu, T. (2022). Yolk-shelled Co@SiO₂@mesoporous carbon microspheres: Construction of multiple heterogeneous interfaces for wide-bandwidth microwave absorption. *J. Colloid Interface Sci.* 607, 1540–1550. doi:10.1016/j.jcis.2021.09.028
- Wang, J., Zhu, P., Wang, J., Ho, S. L., and Tan, J. (2016). Interchange core/shell assembly of diluted magnetic semiconductor CeO₂ and ferromagnetic ferrite Fe₃O₄ for microwave absorption. *AIP Adv.* 7, 055811. doi:10.1063/1.4973204
- Wang, K. J., Ye, Z. W., Li, X. Q., and Yang, J. (2022). Nanoporous resorcinol-formaldehyde based carbon aerogel for lightweight and tunable microwave absorption. *Mater. Chem. Phys.* 278, 125718. doi:10.1016/j.matchemphys.2022.125718
- Wang, L., Bai, X., Wen, B., Du, Z., and Lin, Y. (2019). Honeycomb-like Co/c composites derived from hierarchically nanoporous zif-67 as a lightweight and highly efficient microwave absorber. *Compos. Part B Eng.* 166, 464–471. doi:10.1016/j.compositesb.2019.02.054
- Wang, T., Chen, G., Zhu, J. H., Gong, H., Zhang, L., and Wu, H. (2021). Deep understanding of impedance matching and quarter wavelength theory in electromagnetic wave absorption. *J. Colloid Interface Sci.* 595, 1–5. doi:10.1016/j.jcis.2021.03.132
- Wang, Y., Gao, X., Lin, C., Shi, L., and Wu, G. (2019). Metal organic frameworks-derived Fe-Co nanoporous carbon/graphene composite as a high-performance electromagnetic wave absorber. *J. Alloys Compd.* 785, 765–773. doi:10.1016/j.jallcom.2019.01.271
- Wang, Y., Gao, X., Wu, X., Zhang, W., Luo, C., and Liu, P. (2019). Facile design of 3d hierarchical NiFe₂O₄/N-GN/ZnO composite as a high performance electromagnetic wave absorber. *Chem. Eng. J.* 375, 121942. doi:10.1016/j.cej.2019.121942
- Wang, Y. Y., Zhu, J. L., Li, N., Shi, J. F., Tang, J. H., Yan, D. X., et al. (2022). Carbon aerogel microspheres with *in-situ* mineralized TiO₂ for efficient microwave absorption. *Nano Res.* 15, 7723–7730. doi:10.1007/s12274-022-4494-0
- Wu, L. H., Liu, X., Wan, G. P., Peng, X., He, Z., Shi, S., et al. (2022). Ni/CNTs and carbon coating engineering to synergistically optimize the interfacial behaviors of tio 2 for thermal conductive microwave absorbers. *Chem. Eng. J.* 448, 137600. doi:10.1016/j.cej.2022.137600
- Wu, W. T., Xu, R., Zhou, Y. M., He, M., Lu, P., Wang, R., et al. (2021). Biomimetic 3d coral reef-like GO@TiO₂ composite framework inlaid with TiO₂-C for low-frequency electromagnetic wave absorption. *Carbon* 178, 144–156. doi:10.1016/j.carbon.2020.11.085
- Wu, Y., Shu, R., Shan, X., Zhang, J., Shi, J., Liu, Y., et al. (2020). Facile design of cubic-like cerium oxide nanoparticles decorated reduced graphene oxide with

enhanced microwave absorption properties. *J. Alloys Compd.* 817, 152766. doi:10.1016/j.jallcom.2019.152766

Wu, Y., Shu, R., Zhang, J., Sun, R., Chen, Y., and Yuan, J. (2019). Oxygen vacancy defects enhanced electromagnetic wave absorption properties of 3d net-like multi-walled carbon nanotubes/cerium oxide nanocomposites. *J. Alloys Compd.* 785, 616–626. doi:10.1016/j.jallcom.2019.01.227

Xie, P. T., Li, H. Y., He, B., Dang, F., Lin, J., Fan, R., et al. (2018). Bio-gel derived nickel/carbon nanocomposites with enhanced microwave absorption. *J. Mat. Chem. C Mat.* 6, 8812–8822. doi:10.1039/c8tc02127a

Xing, H., Yin, Q., Liu, Z., and Wang, L. (2017). Excellent microwave absorption behaviors of polyaniline composites containing CeO₂ nanorods in the x-band. *Nano* 12, 1750047. doi:10.1142/s1793292017500473

Xu, J. L., Qi, X. S., Sun, Y., Wang, Z., Liu, Y., Luo, C., et al. (2018). Tuning the electromagnetic synergistic effects for enhanced microwave absorption via magnetic nickel core encapsulated in hydrogenated anatase TiO₂ shell. *ACS Sustain. Chem. Eng.* 6, 12046–12054. doi:10.1021/acssuschemeng.8b02350

Xu, J. L., Sun, L., Qi, X. S., Wang, Z., Fu, Q., and Pan, C. (2019). A novel strategy to enhance the multiple interface effect using amorphous carbon packaged hydrogenated tio₂ for stable and effective microwave absorption. *J. Mat. Chem. C Mat.* 7, 6152–6160. doi:10.1039/c9tc00483a

Xu, L. L., Tao, J. Q., Zhang, X. F., Yao, Z., Zavabeti, A., and Zhou, J. (2022). Co@N-doped double-shell hollow carbon via self-templating-polymerization strategy for microwave absorption. *Carbon* 188, 34–44. doi:10.1016/j.carbon.2021.11.043

Yang, X., Sun, X., Rauf, M., Mi, H., Sun, L., Deng, L., et al. (2020). N-doped porous tremella-like Fe₃C/Ce electrocatalysts derived from metal-organic frameworks for oxygen reduction reaction. *Dalton Trans.* 49, 797–807. doi:10.1039/c9dt03923f

Zhang, X., Wang, J., Su, X., and Huo, S. (2019). Facile synthesis of reduced graphene oxide-wrapped cnfs with controllable chemical reduction degree for enhanced microwave absorption performance. *J. Colloid Interface Sci.* 553, 402–408. doi:10.1016/j.jcis.2019.06.055

Zhang, Z., Tan, J. W., Gu, W. H., Zhao, H., Zheng, J., Zhang, B., et al. (2020). Cellulose-chitosan framework/polyaniline hybrid aerogel toward thermal insulation and microwave absorbing application. *Chem. Eng. J.* 395, 125190. doi:10.1016/j.cej.2020.125190

Zhao, S. Z., Kang, D. J., Liu, Y. P., Wen, Y., Xie, X., Yi, H., et al. (2020). Spontaneous formation of asymmetric oxygen vacancies in transition-metal-doped CeO₂ nanorods with improved activity for carbonyl sulfide hydrolysis. *ACS Catal.* 10, 11739–11750. doi:10.1021/acscatal.0c02832

Zhou, M., Lu, F., Lv, T. Y., Yang, X., Xia, W., Shen, X., et al. (2015). Loss mechanism and microwave absorption properties of hierarchical nico₂o₄ nanomaterial. *J. Phys. D. Appl. Phys.* 48, 215305. doi:10.1088/0022-3727/48/21/215305

Zhou, P. P., Zhang, J., Zhu, H. L., Wang, L., Wang, X., Song, Z., et al. (2020). Silica-modified ordered mesoporous carbon for optimized impedance-matching characteristic enabling lightweight and effective microwave absorbers. *ACS Appl. Mat. Interfaces* 12, 23252–23260. doi:10.1021/acсами.9b23287